JOURNAL OF AIRCRAFT
Vol. 43, No. 5, September–October 2006

Study of Delayed-Detached Eddy Simulation with Weakly Nonlinear Turbulence Model

Zhixiang Xiao,* Haixin Chen,† Yufei Zhang,‡ Jingbo Huang,‡ and Song Fu§
Tsinghua University, 100084 Beijing, People's Republic of China

DOI: 10.2514/1.20127

This paper presents a parallel computation with hybrid Reynolds-averaged Navier–Stokes and large eddy simulation methods. Two types of hybrid approaches, referred to as detached eddy simulation and delayed-detached eddy simulation, are investigated through introducing length scales into the weakly nonlinear k–ω turbulence model. Before the implementation of hybrid methods, the baseline weakly nonlinear model and k–ω shear-stress-transport model are validated in the transonic RAE-2822 airfoil and ONERA-M6 wing cases. The numerical results show satisfactory agreement with the available experimental data. The Reynolds-averaged and hybrid methods based on the weakly nonlinear turbulence model are then applied to calculate the high Reynolds number transonic separation flows around NASA TN D-712 wing fulesage For the higher angle of attack case ($\alpha = 26.2$ deg), both hybrid methods deliver good results when compared with the experiment; for the moderate angle of attack case ($\alpha = 12.5$ deg), the results obtained with the delayed detached eddy simulation are satisfactory, whereas the starting point of the wing vortex breakdown predicted with the detached eddy simulation is too far upstream.

I. Introduction

THREE-DIMENSIONAL (3-D) flow separation around aircrafts at high angles of attack (AOA) has been an interesting and challenging topic in fluid mechanics. Undesired effects, such as loss of lift, increase in drag, amplification of unsteady pressure fluctuations, and uncontrollable abrupt moment change, are always accompanying the separation at high incidence. In 3-D transonic separating flows, the flow features are generally sensitive to the geometry, surface roughness, AOA, Mach number, Reynolds number, and so on. The generation, development, evolution, and breakdown of the vortices and their interaction between shock wave, boundary layer, wake, or other vortices heavily influence the performance of aircrafts. With extremely complex flow patterns, the 3-D separating flows give rise to great challenge to the experimental devices, numerical models, and analysis methodology.

With the rapid development of computer and numerical methods, computational fluid dynamics (CFD) has gradually been widely used in the aircraft design. Currently, the CFD approaches, even for the prediction of unsteady separation flows, are mainly based on Reynolds-averaged Navier–Stokes (RANS) equations. In fact, adequate accuracy and efficiency for steady flows without massive separation or flow recirculation can be obtained using RANS methods with appropriate turbulence models. On the other hand, it is very difficult to find a universal RANS turbulence model that can be reliably applied to the flows with massive separations and multicomponent interferences.

In this aspect, the relatively poor performance of RANS has motivated the increasing application of large eddy simulation (LES). LES is believed to be able to provide accurate turbulent flow simulation at only a fraction of the cost of the direct numerical simulation (DNS). It is a powerful tool for resolving the large, energy-containing scales of motion that are typically dependent on geometry and boundary conditions; the small scale motions are nearly homogeneous and are treated with subgrid scale models.

However, when LES is applied to boundary layers, the overall computational cost does not differ significantly from that of DNS. The "large eddies" close to the solid wall are physically small in scale. Additional empiricism is required in the treatment of the high Reynolds number boundary layer. The subgrid models for the compressible boundary layer are not well developed and require further improvement.

To overcome the deficiencies of RANS and LES, an alternative modeling strategy of turbulence flows, often called the hybrid RANS/LES methods, has been proposed recently for predicting the unsteady and geometry-dependent separating flows. Such hybrid methods combine a high-efficiency turbulence model near the wall where turbulence is dominated by small scale motion with an LES-type treatment for the large scale motion in the core flow region far away from the wall.

Several kinds of hybrid RANS/LES methods have been proposed in the recent decade. The first hybrid method, named as the detached eddy simulation (DES [1]), was developed by Spalart. Here, the distance d from the nearest wall in the Spalart–Allmaras (S-A) [2] model is replaced with $\tilde{d} = \min(d, C_{\mathrm{DES}}\Delta)$. Strelets [3] proposed a DES-type hybrid method based on Menter's k–ω shear-stress-transport model (SST [4]) through the modification of the turbulent length scale L_t in the turbulence kinetic energy transport equation such that $\tilde{L}_t = \min(L_t, C_{\mathrm{DES}}\Delta)$. Davidson [5] combined a one-equation subgrid model with a k–ω model to simulate the recirculation flows. Baurle [6] developed a type of hybrid RANS/LES method for supersonic cavity flows that employs a flow dependent blending function to shift the closure from RANS in the near-wall region to the LES in the outer part of the boundary layer and regions of local separation. Menter [7] developed the delayed-DES (DDES) method to reduce the grid dependency of the DES limiter on the RANS part of the boundary layer. Recently, to overcome the drawback in the original DES, which may for instance prematurely shift the model from RANS to LES because of the local grid refinement in any direction, Deck [8] proposed a zonal-DES method and applied it to predict the supersonic base flow and three-element airfoil flows. Until now, the DES [9–14] based on the S-A model is by far still the most widely used hybrid RANS/LES method.

The core idea of the hybrid methods is the combination of the RANS near the wall with LES in the separation region. The fundamental turbulence models still significantly affect the predicted flow characteristics for the aircraft application. To construct the hybrid RANS/LES methods rationally, it is generally hoped

Received 18 September 2005; revision received 21 November 2005; accepted for publication 23 November 2005.

*Researcher Assistant, School of Aerospace Engineering.
†Associated Professor, School of Aerospace Engineering.
‡Ph.D. Candidates, School of Aerospace Engineering.
§Corresponding author, Professor, School of Aerospace Engineering, Senior Member AIAA.

that the turbulence model has good numerical properties and be *low-Reynolds number* in nature to resolve the near-wall turbulence characteristics. The two-equation k–ω model, for its favorable numerical aspects, is commonly taken as an appropriate choice despite the fact that the original k–ω model proposed by Wilcox [15] suffers from undesirable free-stream dependence. Menter [4] developed a hybrid two-equation SST model through coupling the k–ω model in the near-wall region with the less free-stream dependent k-ε model outside the boundary layer. This model considers the transport of principal turbulent shear stress and shows good capability for adverse pressure gradients flows. Recently, nonlinearity in eddy viscosity modeling has been reconsidered in the view of realizability, which is not satisfied by any linear eddy viscosity formulation based on Boussinesq's assumption [16]. It is found that certain weakly nonlinear eddy viscosity formulations can effectively further improve the model's performance under adverse pressure gradients, especially for the flows with shock-wave/ boundary-layer interaction [17].

In this paper, the capability of the k–ω model with weakly nonlinear eddy viscosity formulation (Wilcox–Durbin, WD+ [17,18]) is first demonstrated through predicting the transonic RAE-2822 airfoil and ONERA-M6 wing cases, both with shock-wave/ boundary-layer interactions. The results computed with the SST model are also presented for comparison.

Xiao [19] predicted the 3-D transonic separation flows around the NASA TN D-712 wing-fuselage standard model [20] in a RANS way using the two-equation k–g low-Reynolds model without any wall distance parameter. The present work employs the same configuration at moderate and high AOAs and focuses on the prediction of the vortex structures and the wing-body interference with unsteady-RANS, DES, and DDES methods based on the WD+ model.

For the solution of the NS equations, several numerical schemes, such as the Roe-type [21] flux-difference-splitting scheme together with the Radespiel and Swanson (RS) entropy fix [22] and second-order implicit lower–upper symmetric-Gauss–Seidel (LU-SGS) with pseudotime subiteration (τTS) time-marching method [23], are applied. The turbulence model equations are solved, uncoupled with the mean flow equations, using the LU-SGS method.

II. Turbulence Models, DES and DDES Methods

In the present work, the k–ω family turbulence models are considered, and C_μ is incorporated into the definition of ω.

A. Original Wilcox's k–ω Model

The original k-ω model developed by Wilcox [15] is given as

$$\frac{\partial \rho k}{\partial t} + \frac{\partial}{\partial x_j}\left(\rho u_j k - (\mu + \sigma_k \mu_t)\frac{\partial k}{\partial x_j}\right) = \tau_{ij} S_{ij} - \beta^* \rho k \omega \tag{1}$$

$$\frac{\partial \rho \omega}{\partial t} + \frac{\partial}{\partial x_j}\left(\rho u_j \omega - (\mu + \sigma_\omega \mu_t)\frac{\partial \omega}{\partial x_j}\right) = P_\omega - \beta \rho \omega^2 \tag{2}$$

where $P_\omega \equiv 2\gamma\rho(S_{ij} - \omega S_{kk}\delta_{ij}/3)S_{ij} \approx \gamma\rho\Omega^2$; S_{ij} is the strain rate which is defined as $(\partial u_i/\partial x_j + \partial u_j/\partial x_i)/2$; and Ω is the magnitude of the vorticity. The constants are $\sigma_k = \sigma_\omega = 0.5$, $\gamma = 5/9$, $\beta^* = 0.09$, and $\beta = 3/40$. The eddy viscosity is defined as

$$\mu_{t,\text{Wilcox}} = \rho k/\omega \tag{3}$$

Equation (3) was originally designed to accurately predict the boundary-layer flows with a zero pressure gradient.

B. The k–ω WD+ Model

The linear eddy viscosity definition in Eq. (3) is known to be inadequate in the prediction of flow under adverse pressure gradients. The weakly nonlinear correction is to produce asymptotic behavior of C_μ when S_{ij} approaches infinity. In the WD+ model, the equations remain the same as those in the original k–ω model. A new formulation of μ_t with weakly nonlinear correction is given as

$$\mu_{t,\text{WD+}} = \min\left[\frac{\rho k}{\omega}; \frac{\rho a_1 k}{\sqrt{(\Omega^2 + \tilde{S}^2)/2}}\right] \tag{4}$$

where $\tilde{S}^2 = 2S_{ij}S_{ji} - \frac{2}{3}S_{kk}$.

C. The k–ω SST Model

This zonal model uses Wilcox's k–ω model, which is well behaved near solid walls and needs no low-Reynolds number corrections. At the same time, it combines with the standard k–ε model (reformulated in a k–ω style), which is relatively insensitive to free-stream values in the outer edge of the boundary and free stream. The switching is realized by a flow dependent blending function. The SST model also limits the eddy viscosity by forcing the turbulent shear stress to be bounded by a constant times the turbulent kinetic energy inside boundary layers (a realizability constraint). This modification improves the model's performance on flows with strong adverse pressure gradients and separation.

The SST turbulence model equations are given as

$$\frac{\partial \rho k}{\partial t} + \frac{\partial}{\partial x_j}\left(\rho u_j k - (\mu + \sigma_k \mu_t)\frac{\partial k}{\partial x_j}\right) = \tau_{ij} S_{ij} - \beta^* \rho k \omega \tag{5}$$

$$\frac{\partial \rho \omega}{\partial t} + \frac{\partial}{\partial x_j}\left(\rho u_j \omega - (\mu + \sigma_\omega \mu_t)\frac{\partial \omega}{\partial x_j}\right) = P_\omega - \beta \rho \omega^2 + 2(1 - F_1)\frac{\rho \sigma_{\omega 2}}{\omega}\frac{\partial k}{\partial x_j}\frac{\partial \omega}{\partial x_j} \tag{6}$$

where

$$F_1 = \tanh\left\{\left[\min\left(\max\left(\frac{\sqrt{k}}{0.09\omega d}; \frac{500\mu}{\rho d^2 \omega}\right); \frac{4\rho\sigma_{\omega 2} k}{CD_{k\omega} d^2}\right)\right]^4\right\}$$

and the cross diffusion

$$\text{CD}_{k\omega} = \max\left(\frac{2\rho\sigma_{\omega 2}}{\omega}\frac{\partial k}{\partial x_j}\frac{\partial \omega}{\partial x_j}; 10^{-20}\right)$$

The constants are $a_1 = 0.31$, $\beta^* = 0.09$, and $\kappa = 0.41$; d is the distance from the nearest wall. Some other constants are calculated from $\phi = F_1\phi_1 + (1 - F_1)\phi_2$, where the ϕ's are constants: $\sigma_{k1} = 0.85$, $\sigma_{\omega 1} = 0.5$, $\beta_1 = 0.075$, $\gamma_1 = \beta_1/\beta^* - \sigma_{\omega 1}\kappa^2/\sqrt{\beta^*} = 0.553$; $\sigma_{k2} = 1.0$, $\sigma_{\omega 2} = 0.856$, $\beta_2 = 0.0828$, $\gamma_2 = \beta_2/\beta^* - \sigma_{\omega 2}\kappa^2/\sqrt{\beta^*} = 0.44$.

The eddy viscosity of the SST model is given by

$$\mu_{t,\text{SST}} = \min\left[\frac{\rho k}{\omega}; \frac{\rho a_1 k}{\Omega F_2}\right] \tag{7}$$

where

$$F_2 = \tanh\left\{\left[\max\left(2\frac{\sqrt{k}}{0.09\omega d}; \frac{500\mu}{\rho d^2 \omega}\right)\right]^2\right\}$$

is another blending function. In Eq. (7), the eddy viscosity of the SST model, which is in a form similar to Eq. (4), also includes a nonlinear effect. Therefore, the SST model can be thought of as a weakly nonlinear turbulence model, too.

D. DES and DDES Methods

The motivation of the hybrid RANS/LES method is to combine the best features of both LES and RANS methods. RANS can predict attached flows very well with relatively less computation cost. LES has demonstrated its ability to compute the separated flows accurately but with more computation cost for boundary-layer flows.

The Reynolds-stress or subgrid stress tensor term is defined as

$$\tau_{ij} = -\overline{\rho u_i' u_j'} \tag{8}$$

where u_i' denotes the fluctuating velocity u_i component and the overbar represents the mean or the large-scale value.

The stress tensor in DES and DDES is modeled with the LES-type Smagorinsky [24] subgrid model, that is,

$$\tau_{ij} = 2\rho\nu_{\text{Sma}}S_{ij}, \qquad \nu_{\text{Sma}} = C_s\Delta^2\tilde{S} \tag{9}$$

where C_s is the model constant ranging from 0.01 to 0.05; Δ is the grid scale.

To construct DES-type hybrid method based on two-equation models, some transformation is adopted for the dissipation terms in the turbulence kinetic energy transport equation. After introducing the length scale, this equation is written as

$$\frac{\partial(\rho k)}{\partial t} + \frac{\partial}{\partial x_j}\left(\rho u_j k - (\mu + \sigma_k\mu_t)\frac{\partial k}{\partial x_j}\right) = \tau_{ij}S_{ij} - \beta^*\rho k\omega F_{\text{DES}} \tag{10}$$

where F_{DES} is the hybrid function given as $F_{\text{DES}} = \max[(1 - F_{\text{SST}})\cdot L_t/(C_{\text{DES}}\Delta); 1]$; the length scale L_t is defined as $L_t = k^{1/2}/(\beta^*\omega)$; $C_{\text{DES}} = 0.78$; F_{SST} can be taken as 0, F_1 and F_2, where F_1 and F_2 are the two blending functions in the SST model. If $F_{\text{SST}} = 0$, the hybrid method returns to the Strelets-type DES method. If $F_{\text{SST}} = F_1$ or F_2, this kind of hybrid method is called as the delayed-DES [7] method. In this paper, F_{SST} is taken as F_2. The ω equation and the eddy viscosity definition are the same as that in the WD+ model.

In the Strelets-type DES method (i.e., $F_{\text{SST}} = 0$), when $L_t < C_{\text{DES}}\Delta$, and $F_{\text{DES}} = 1$, the hybrid method acts in the WD+ mode; when $L_t > C_{\text{DES}}\Delta$, the method acts in a Smagorinsky LES mode. When the turbulence production is balanced with the dissipative term, $P_k = \rho\nu_t\tilde{S}^2 = D_k = \rho k^{3/2}/L_t$, $k = \beta^*L_t^2\tilde{S}^2$, and $L_t = C_{\text{DES}}\Delta$. Then the eddy viscosity is given as

$$\nu_t = (\beta^*)^{3/2}(C_{\text{DES}}\Delta)^2\tilde{S} \propto \Delta^2\tilde{S} \tag{11}$$

From Eq. (11), the eddy viscosity is similar to that of the Smagorinsky model. When the grid is locally refined, the hybrid method will act as in a LES mode.

III. Numerical Methods

The computations in this paper are all based on a compressible solver using the Roe flux-difference splitting scheme with 3rd-order monotone upstream centered scheme for conservation laws (MUSCL) and a RS entropy fix in a cell-centered finite-volume formulation. A modified fully implicit LU-SGS with Newton-like subiteration in pseudotime is taken as the time-marching method when solving the mean flow equations and the turbulence model equations. Global nondimensional time stepping ($\Delta t = 0.005$) is implemented to capture the unsteady properties of the separation flows. It indicates that the RANS method here is the unsteady RANS. Implicit residual smoothing [25] is employed to accelerate the convergence in the computational procedure. The approach is parallelized using domain decomposition and message-passing-interface strategies for the platform on PC clusters with 64-bit AMD Athlon 3000+.

A. RS Entropy Fix

The main drawback in the Roe linearization is the violation of entropy at sonic rarefactions and near the wall where the eigenvalues approach zero. In addition, there are some other pitfalls, such as the formation of Carbuncle shocks, strong odd-even coupling of pressure and density resulting in the breakdown of grid aligned planar shocks, negative internal energy, and kinked Mach stems. To avoid the nonphysical solution, entropy fix often needs to be added. The early Harten's entropy fix invariably cured these deficiencies when the fix was applied to the linear waves. The present entropy fix, proposed by Radespiel and Swanson [22], takes into account the effects of the high aspect ratios of the viscous grids near the wall and therefore has a smaller effect on the viscous flow simulation accuracy.

B. LU-SGS-τTS Time-Marching Method

The original LU-SGS scheme, which was developed by Yoon and Jameson [26], is unconditionally stable and completely vectorizable. However, the explicit treatment of the viscous terms, the approximation of the flux Jacobian matrices, and the linearization procedure decrease its temporal accuracy. To achieve higher accuracy in time, a Newton-like subiteration is implemented with pseudotime [23]. The time-marching method in this paper can be written as

$$(L + D)D^{-1}(D + U)\Delta\bar{Q}^m = -(3\bar{Q}^m_{i,j,k} - 4\bar{Q}^n_{i,j,k} + \bar{Q}^{n-1}_{i,j,k})/2 - \Delta t\bar{R}^m_{i,j,k} \tag{12}$$

$L = -\alpha(A^+_{i-1,j,k} + B^+_{i,j-1,k} + C^+_{i,j,k-1})$, $U = \alpha(A^-_{i+1,j,k} + B^-_{i,j+1,k} + C^-_{i,j,k+1})$, and $D = [1.5 + \alpha\chi(\sigma_A + \sigma_B + \sigma_C) + 2\alpha\theta]\times I$ where $\Delta\bar{Q}^m = \bar{Q}^{m+1} - \bar{Q}^m$; $\bar{R}^m_{i,j,k}$ are the residuals of the NS equations; $\alpha = \Delta t/\text{Vol}_{i,j,k}$; $A^\pm$, $B^\pm$, and $C^\pm$ are the matrices of the advective flux in three directions; σ_A, σ_B, and σ_C are the spectral radius in the ξ, η, and ζ directions; χ is a constant, which is set to 1.01; θ is a stable factor which can improve the robustness of the computational procedure and is defined as $2(\mu + \mu_t)/(\rho|\nabla\zeta|^2)\cdot Re$, where Re denotes the Reynolds number.

The initial values for the subiteration are taken as $\bar{Q}^0_{i,j,k} = \bar{Q}^n_{i,j,k}$. Starting with $m = 0$, the sequence of iteration $\bar{Q}^m_{i,j,k}$, $m = 1, 2, 3, \ldots$ converges to $\bar{Q}^{n+1}_{i,j,k}$ until the right-hand unsteady residuals have approached zero.

When $\Delta\bar{Q}^m_{i,j,k} \to 0$, it means that the residuals are converged in the pseudotime. The accuracy of the solution at each physical time step is the accuracy of the discrete unsteady governing equations. That is to say, in the case of convergence, $\bar{Q}^{m+1}_{i,j,k} \to \bar{Q}^{n+1}_{i,j,k}$, and $\bar{R}^{m+1}_{i,j,k} \to \bar{R}^{n+1}_{i,j,k}$, then the following equation is valid:

$$(3\bar{Q}^{n+1}_{i,j,k} - 4\bar{Q}^n_{i,j,k} + \bar{Q}^{n-1}_{i,j,k})/2 + \Delta t\bar{R}^{n+1}_{i,j,k} \to 0 \tag{13}$$

whereas the residual $\bar{R}^{n+1}_{i,j,k} = (\delta\bar{F}^{n+1}_{i,j,k} - \delta\bar{F}^{Vn+1}_{i,j,k}/\text{Re})/\text{Vol}_{i,j,k}$, then Eq. (13) yields a second-order fully implicit scheme in physical time,

$$\text{Vol}_{i,j,k}\frac{3\bar{Q}^{n+1}_{i,j,k} - 4\bar{Q}^n_{i,j,k} + \bar{Q}^{n-1}_{i,j,k}}{2\Delta t} + \delta\bar{F}^{n+1}_{i,j,k} = \frac{1}{\text{Re}}\delta\bar{F}^{Vn+1}_{i,j,k} \tag{14}$$

The computing practices show that the rate of convergence with the pseudotime level is very fast, and only a few subiterations are needed.

C. Boundary Conditions

At far-field boundaries, the 1-D Riemann characteristic analysis is employed to construct a nonreflection boundary condition. For smooth surfaces, no-slip boundary condition is used. Symmetric boundary condition is applied for the half-model. "Ghost cells" are used to treat all kinds of boundary conditions including the boundary of the adjacent zonal domains.

D. Solution Methods of Turbulence Model Equations

The turbulent kinetic energy and specific dissipation rate transport equations are solved, decoupled with the mean flow equations, using the LU-SGS method. The production terms are treated explicitly, lagged in time whereas the destruction and diffusion terms are treated implicitly (they are linearized and a term is brought to the left-hand side of the equations). Treating the destruction terms implicitly helps increase the diagonal dominance of the left-hand side matrix. The advective terms are discretized using second-order upwinding. The diffusive terms are discretized using a second-order central scheme.

IV. Results and Discussion

In this paper, if without notification, x denotes the streamwise direction, z denotes the spanwise direction. B denotes the full span, and the half-span $B/2$ is chosen as the character length for the wing-fuselage TN D-712 model. The grids are generated by solving elliptic equations. Appropriate zonal decomposition and grid topology selection are performed according to the characteristics of the configuration.

To investigate the performance of the WD+ model, transonic flows with shock-wave/boundary-layer interaction past RAE-2822 airfoil and ONERA-M6 wing are first computed. The numerical results with the SST model are also presented for comparison. Then the RANS, DES, and DDES methods based on the WD+ model are illustrated for the transonic separation flows past the TN D-712 fuselage/wing combination.

A. Applications of RANS on SST and WD+ Models

1. RAE-2822 Airfoil

Figure 1 presents the C-type computational grid around the airfoil which consists of 284 (streamwise) × 75 (normal) nodes; the far-field boundary is located at a distance of 15 times the chord length and the distance from the first cell center to the wall is about 1×10^{-5} chord.

Figures 2 and 3 display the pressure and skin-friction coefficients and velocity profiles, which reveal a typical supercritical airfoil flow pattern. For this case, $M_\infty = 0.75$, AOA $= 2.79°$, and the Reynolds number based on the chord is 6.2×10^6. The primary flow features for this case are the shock-wave/boundary-layer interaction and separation behind the shock. The SST and WD+ models in Fig. 2 are both in good agreement with the experimental data. Only the shock is a little behind the measured location. Almost identical extents of the separation zone behind the shock wave are predicted with the two models as shown in the skin-friction coefficient distributions. The velocity profiles on the upper surface in Fig. 3 demonstrate that both models can give very good results whereas the WD+ model's results are inconspicuously better.

2. ONERA-M6 wing

The ONERA-M6 wing is a widely used 3-D test case for the validation of numerical methods and turbulent models. The test case selected here is the $M_\infty = 0.8447$, and the AOA $= 5.06°$ one. The free-stream Reynolds number based on the mean chord is 11.7×10^6. The main difficulties of this case are the presentation of the "γ" shock wave, the interactions of the shock wave and the boundary layer and the separation induced by the strong shock. C-H type grids with 187 (streamwise) × 56 (spanwise) × 65 (normal) nodes and about 1×10^{-5} first wall distance are used.

The pressure coefficients distribution is compared with the wing sections located at $2z/B = 22$, 44, 65, 80, 90, and 95% shown in Fig. 4. From it, two turbulence model's results match the experiment very well and the differences are quite small. It is observed that the predicted shock position with the SST model is just a little more upstream than that of the WD+ model, especially near the wing tip. This is different from the RAE2822 case. In some sense, the difference may reflect the different definition of the eddy viscosity and the closure coefficients in the two models.

Figure 5 shows the surface streamlines and the pressure contour over the upper surface of the M6 wing. It shows that the spanwise flow computed with the SST model is stronger than that of the WD+ model. For example, the spanwise position of the start separation line L1 with the SST model is 0.132, whereas L1 with the WD+ model is 0.172. The saddle point P2 with the SST model is 0.828, and that with the WD+ model is 0.834. At $2z/B = 0.4$, the separation induced by the strong shock ranges streamwise from $2x/B = 0.563$ to 0.615 with the SST model and from $2x/B = 0.566$ to 0.614 with the WD+ model. The separation widths with the two models are 0.052 and 0.048, respectively. The details of L1, P2, and W3 are demonstrated in Table 1.

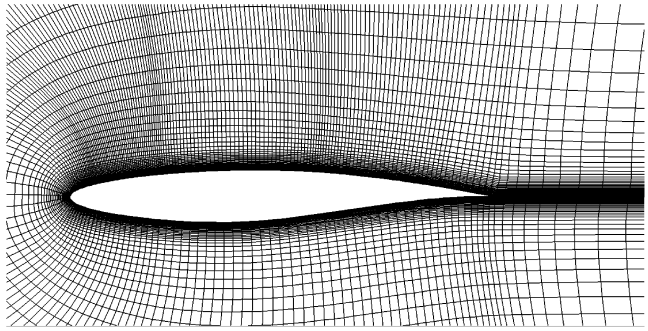

Fig. 1 The grids near the RAE-2822 airfoil.

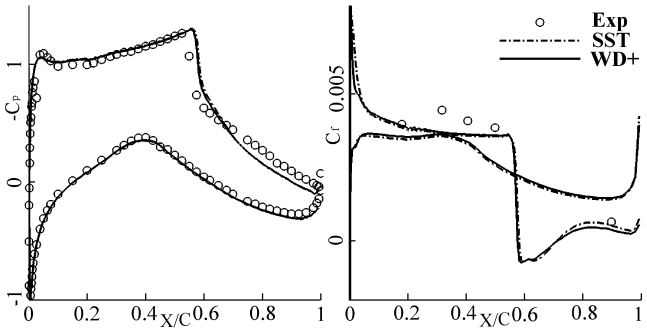

Fig. 2 Comparison on the pressure and skin-friction coefficients.

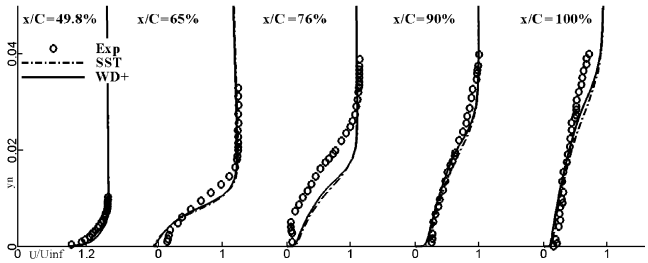

Fig. 3 Comparison on velocity profile at several streamwise positions.

The convergence of maximum and mean residuals with both the SST and the WD+ models are shown in Fig. 6. Both models show very good numerical properties, especially in the 2-D airfoil case.

B. Applications of RANS, DES, and DDES on the WD+ Model

1. NASA TN D-712 Wing-Fuselage Model

This wing-fuselage configuration consists of a low aspect ratio, high swept angle midwing, and a fuselage with pointed nose and boat-tail aft body. Five $161 \times 91 \times 28$ H-H type grid blocks (altogether 2.0 million cells in the whole field, designated grids A) (streamwise/spanwise/normal) are shown in Fig. 7. A coarser grid with fewer normal grids (five $161 \times 91 \times 21$ grid blocks, totally about 1.5 million cells, named grids B) is also generated. Another locally refined grid including $171 \times 91 \times 28$ (about 2.2 million cells, called grids C) is also studied for the effect on grid scales. Figure 8 shows the surface grids of grids A (or B) and C. From it, the difference between grids A (or B) and C is that the wing leading-edge streamwise grids of C are denser than that of A (or B).

The computations are performed for the Mach number 0.9 case. The Reynolds number is 7.5×10^6 (based on the half-span). Results of two AOAs are presented in this paper: one is the AOA $= 12.5$ deg and the other is 26.2 deg. In both cases, the flows are separated with vortices emerging from the wing leading edge or even from the forebody.

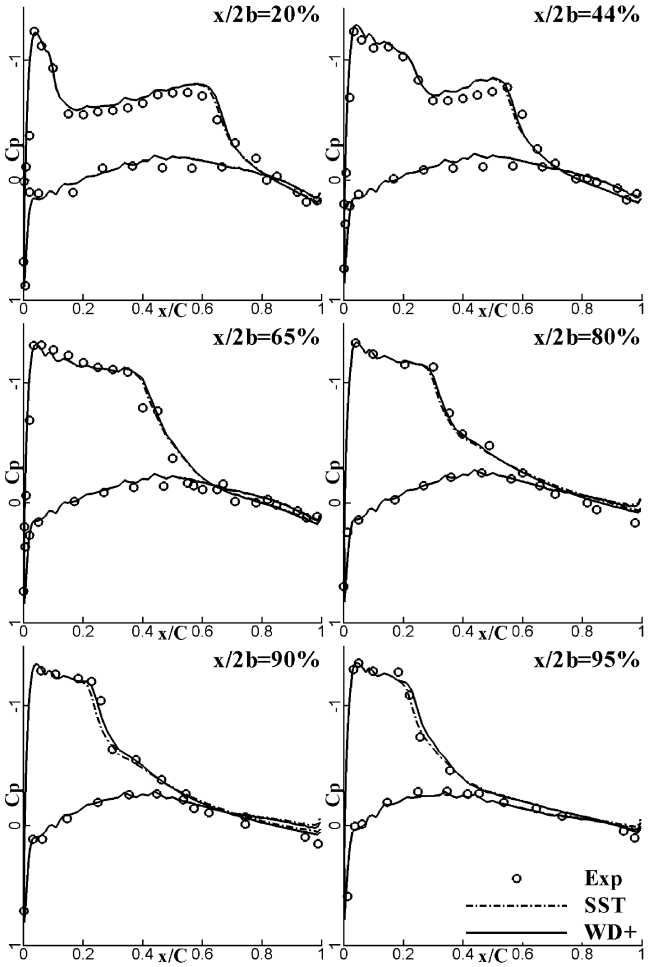

Fig. 4 Comparison on wall-pressure coefficients over wing M6.

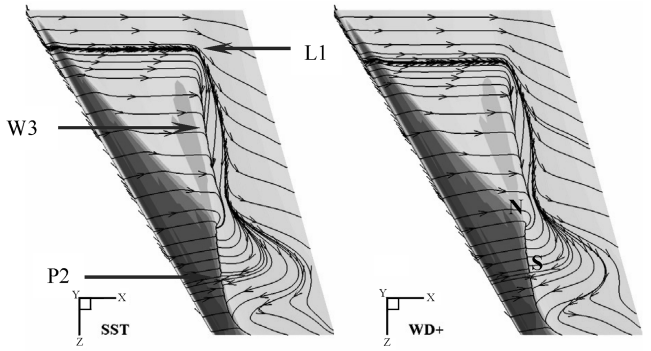

Fig. 5 Surface streamlines and pressure contour computed with SST and WD+ models.

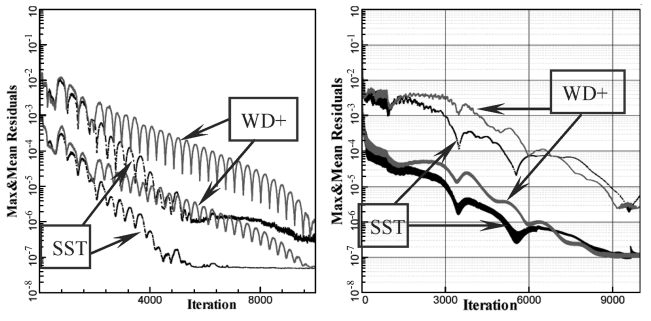

Fig. 6 Convergence of the two models (left: RAE2822; right: M6).

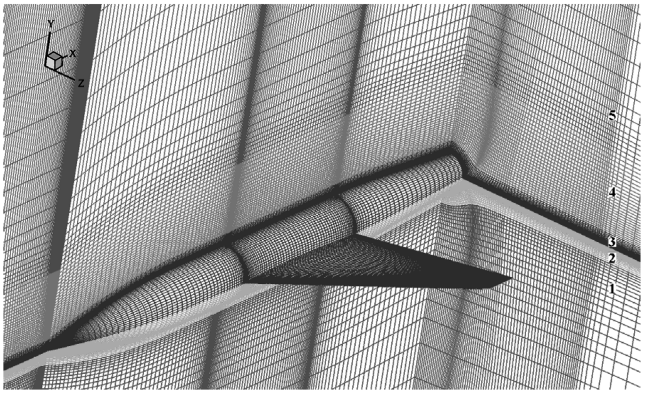

Fig. 7 Grids around NASA TN D-712.

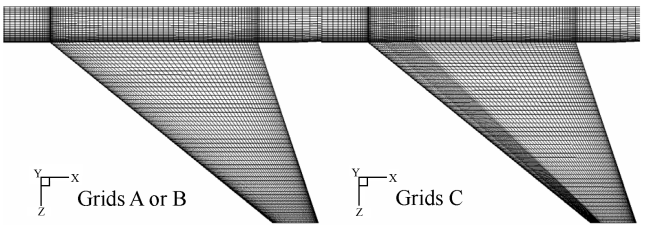

Fig. 8 Original and locally refined grids.

Table 1 Difference between the two models

	Model	X	Z	
L1	SST	——	0.132	
	WD+	——	0.172	
P2	SST	0.608	0.828	
	WD+	0.611	0.834	
W3 at $2z/B = 0.4$	Streamwise	X_{start}	X_{end}	Width
	SST	0.563	0.615	0.052
	WD+	0.566	0.614	0.048

2. Case I: AOA = 12.5 deg

The computational pressure coefficients over the wing are compared with experimental data. Six wing sections located at $2z/B = 16, 25, 40, 60, 75$, and 95% are presented, where the section at $2z/B = 16\%$ is just located at the wing and fuselage junction. Very serious aerodynamic interference between the wing and fuselage can be found on the pressure distribution of the wing root sections at $2z/B = 16$, 25, and 40%. At sections $2z/B \geq 60\%$, the flow is completely separated, and the pressure coefficients on the upper surface almost look like a straight line.

Figure 9 presents the grid effect on the pressure coefficients distribution over the wing computed with RANS based on the WD+ model. The solid, dash-dotted, and dashed lines denote the results based on grids A, B, and C, respectively. All the numerical results can match the experimental data well, whereas the computational pressure coefficients over the upper surface at sections $2z/B = 60$ and 75% are a little lower than that of experiment. There is little difference of pressure on the lower surface of the wing. At the sections near the wing tip, the pressure results do not differ from each other distinctly from the curves. The main difference between the results of grids A and B is the high pressure region's (HPR) position and size on the upper surface of the wing. The HPR position based on grids B is more downstream than that of grids A; and the HPR size of grids B is larger and more noncompact than that of grids A. In addition, the pressure recovery based on grids B is weaker than grids A and experimental data. However, the surface pressure coefficients based on grids A and C show little difference. From this

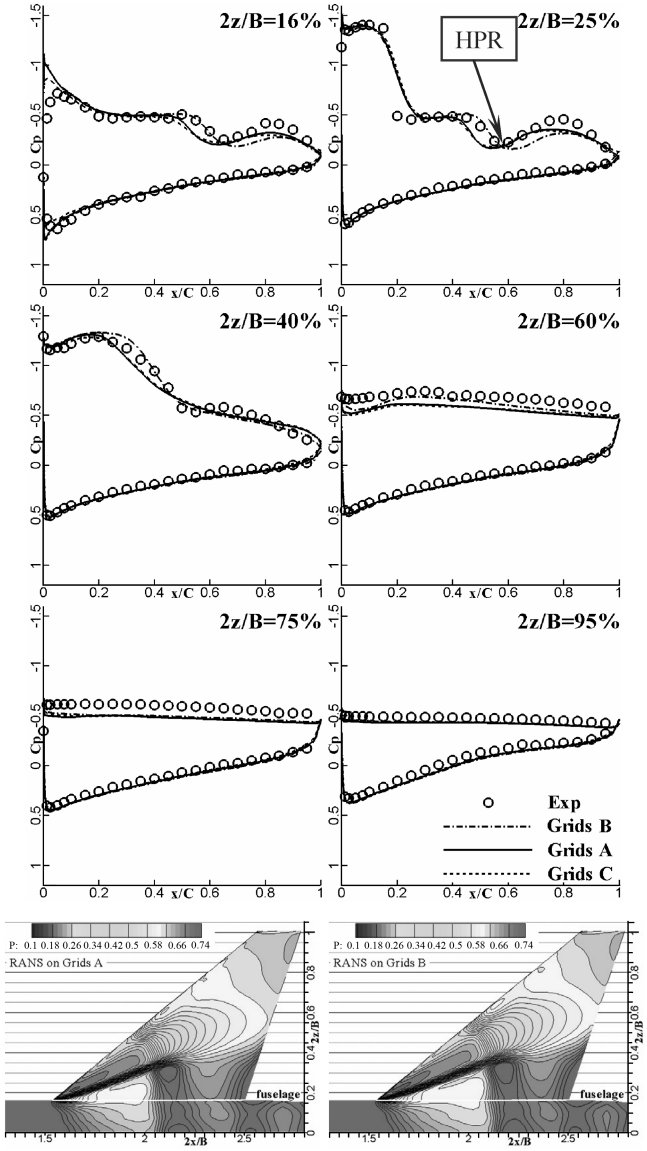

Fig. 9 Comparison on pressure over the wing with different grids.

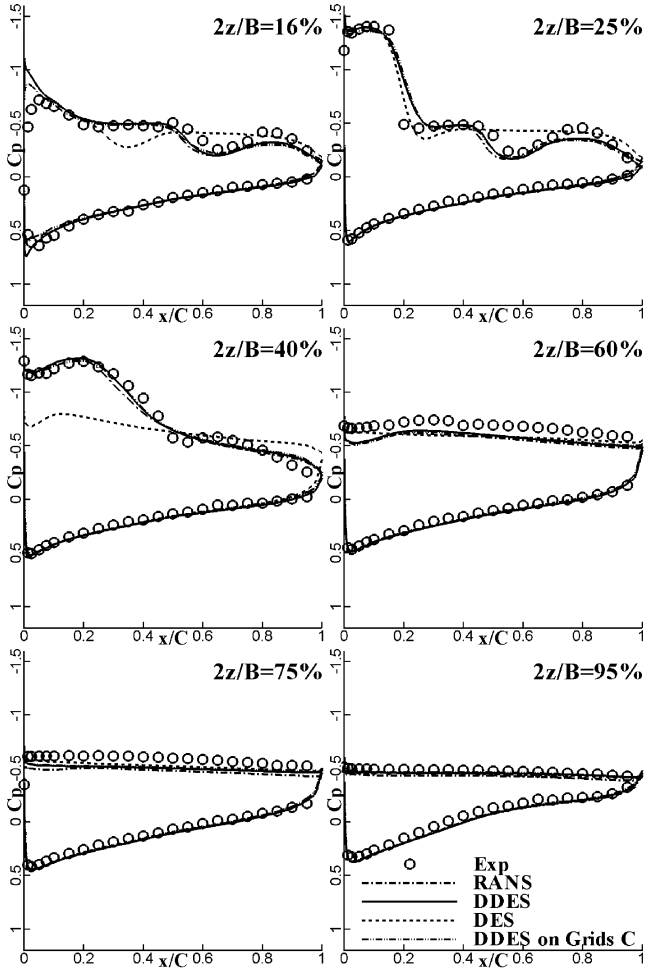

Fig. 10 Comparison on pressure over the wing with RANS, DES, and DDES methods.

figure, it implies that the grids influence on the pressure distribution is different from each other in either normal or streamwise directions. Therefore, grids A are taken as the baseline grids for the DES and DDES methods.

The initial conditions for DES and DDES methods are obtained by solving RANS equations with the WD+ model. The time-averaged pressure coefficients with RANS, DES, and DDES methods are plotted in Fig. 10 (if there is no special explanation, all the following results are time averaged). It is very disappointing that the results with Strelets-type DES show great difference from those of experiment. After study of the 3-D infinite span wing flows with strong adverse pressure, Menter [7] points out that the original DES limiter affects the RANS methods and moves the separation start point upstream relative to the original SST model. In the present study, through analyzing the vortices detached from the leading point of fuselage and wing conjunction (shown in Fig. 11), the main reason which causes the inaccuracy is that the original DES limiter affects the RANS method and moves the start point of the wing vortex breakdown far upstream. (Here, the start point of the wing vortex breakdown in the streamwise direction is at $2x/B = 1.88$ with DES and 2.26 with RANS, respectively.)

In the DDES results, the bad influence of the original DES limiter on the RANS part of the hybrid methods is effectively reduced. The start point of the wing vortex breakdown with DDES is at $2x/B = 2.138$, just a little more upstream than that of the RANS. Moreover, DDES shows some improvement on the position of HPR and matches the experimental pressure coefficients distribution better than RANS from Fig. 10. The start point of vortex breakdown at $2x/B = 2.140$ based on grids C does not differ from that of grids A. It indicates that the DDES can effectively eliminate the locally refined grids effects. Little difference exists between the pressure coefficients, which are also presented in Fig. 10, on the baseline grids A and the locally refined grids C.

In Fig. 11, the total pressure slice over the wing at the section of $2x/B = 2.167$ shows a different shape and size with different methods. The vortex with RANS is compressed and the size is small; however, all those with the hybrid methods are large and round. It is also indicated that the vortex with the hybrid methods undergoes breakdown whereas that with RANS does not.

Figure 12 demonstrates the cross flow pattern at section $2x/B = 2.167$. Two detached vortices are presented; one is emerged from the fore fuselage and the other is from the wing and fuselage conjunction point. At this section, the most distinct difference between RANS and DDES is the vortex shape and size over the wing. As aforementioned, the vortex with DDES undergoes breakdown whereas the vortex with RANS stays very strong.

3. Case II: AOA = 26.2 deg

At higher alpha, the flow over the upper surface of the TN D-712 is almost entirely separated. The vortices from the fore fuselage and the wing leading edge are much stronger than those in case I.

The pressure coefficients with RANS, DES, and DDES are shown in Fig. 13. From this figure, the interference between the fuselage and the wing looks weaker than that in case I. The upper surface pressure coefficients with RANS are a little lower than the experiment,

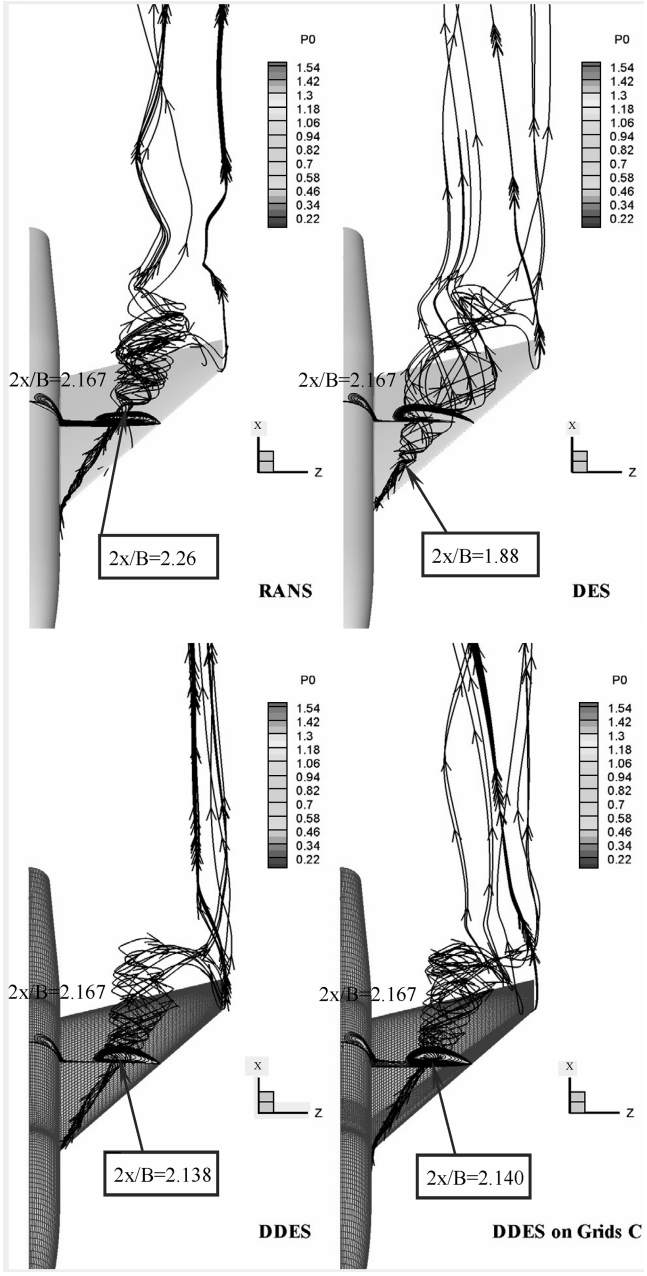

Fig. 11 Comparison on the vortex over the wing with RANS, DES, and DDES methods.

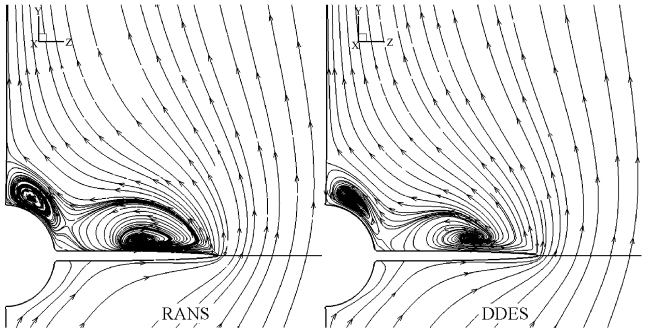

Fig. 12 Comparison of streamlines with RANS and DDES.

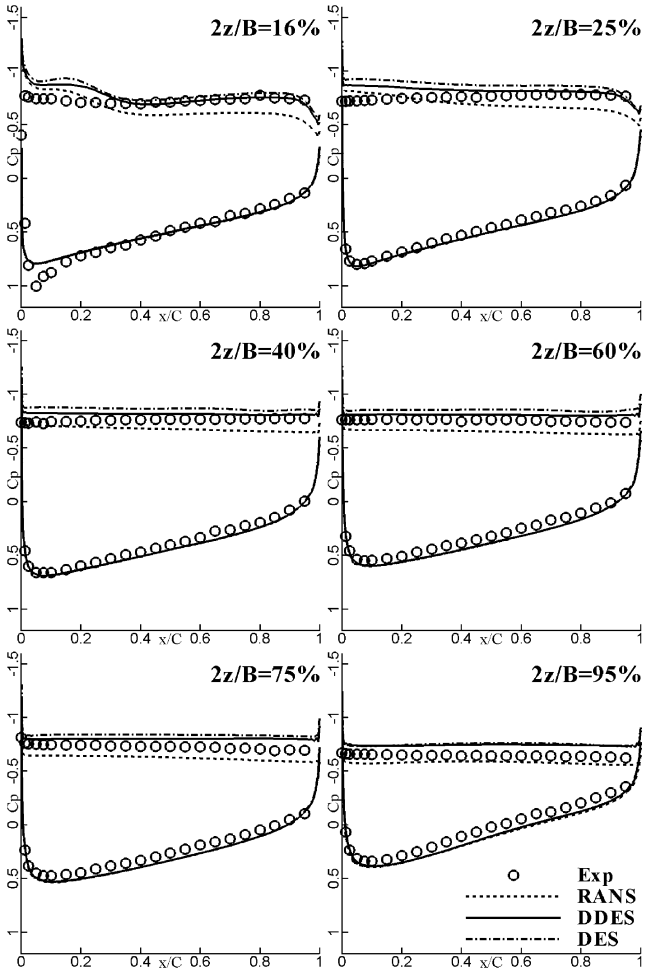

Fig. 13 Comparison on pressure over the wing with RANS, DES, and DDES methods.

whereas those with DES are a little higher; DDES, whose values are between the DES and RANS, shows the best agreement with the experiment.

The streamlines on the upper surface of TN D-712 are shown in Fig. 14. The flow patterns on the upper surface are very complex. Primary and secondary separation and the reattachment lines on the fore fuselage are clearly visible. The primary reattachment line lies in the flow symmetric plane. On the upper surface of the wing, the flow is almost totally separated. Near the top point of the junction, a helix point is predicted with all methods. Differing from the other two methods, another distinct helix point near the middle part of the wing is predicted with DES.

The vortices using hybrid methods over the wing and fuselage are shown in Fig. 15. Little difference exists between DES and DDES. The vortices detached from the fore fuselage are merged into the wing leading-edge vortices, by which the separation of the whole upper wing is induced. Some typical instantaneous vortices contour surface with DES and DDES methods are shown in Fig. 16. DDES reveals more flow structures than those with DES.

V. Conclusion

The weakly nonlinear eddy viscosity formulated k-ω WD+ model can predict the transonic shock-wave and boundary-layer interaction flows very well when compared with another widely used SST model.

RANS, DES, and DDES methods based on the WD+ model are implemented to predict the transonic vortice flows accounting for the effect on the interference of the different components past the NASA TN D-712 wing-fuselage model at moderate AOA (12.5 deg). RANS based on both 2.0 million grids and 1.5 million grids can predict the interference between the wing and fuselage very well; the DES predicted start point of the wing vortex breakdown is too upstream than the experiment and RANS results. DDES can give more reliable flow patterns on both the vortices structures and surface pressure distribution over the wing even based on the locally refined grids C.

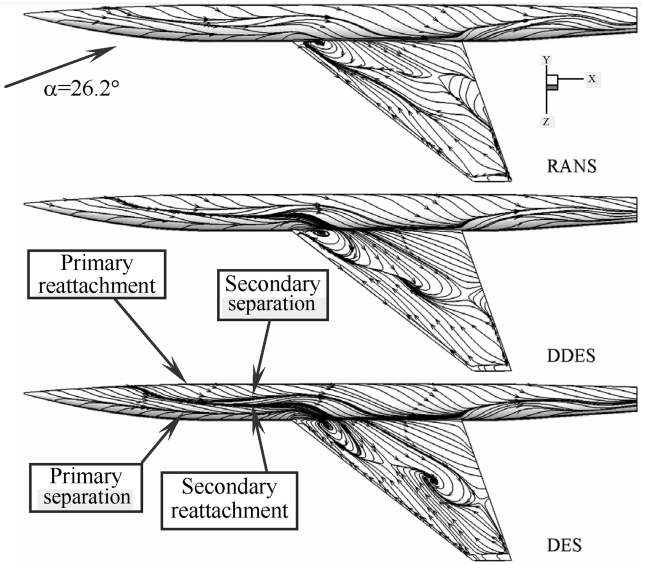

Fig. 14 Comparison of streamlines on the upper surface.

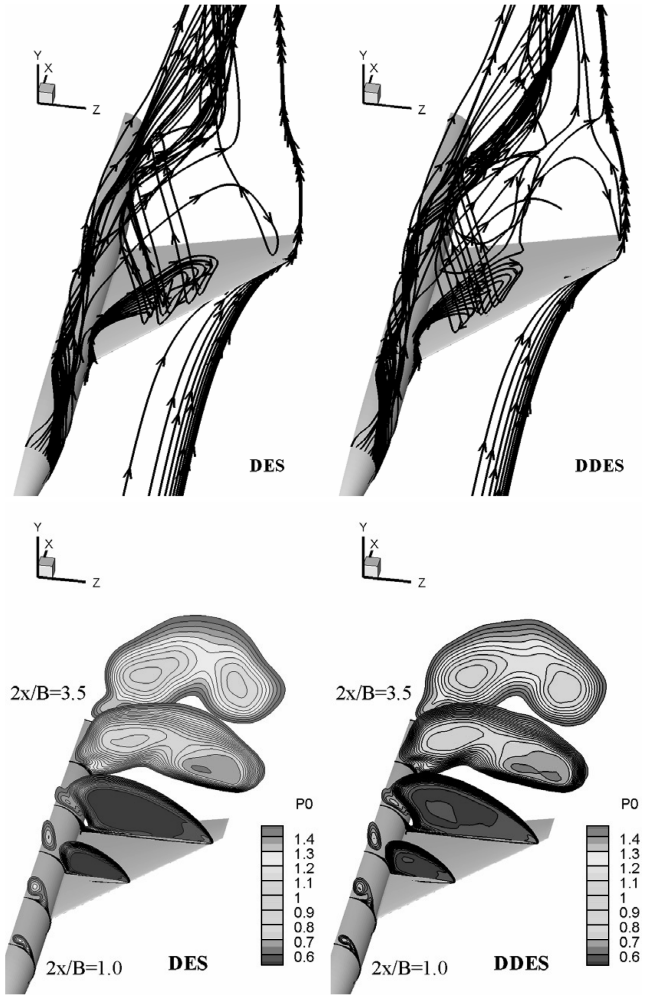

Fig. 15 Comparison of the vortices above the fuselage and wing.

At higher AOA (26.2 deg), RANS underpredicts the pressure coefficients on the wing whereas DES overpredicts. However, the results with DDES lie between those with RANS and DES and match the experiment well. Furthermore, DDES reveals more detailed flow information and vortices structures than those with DES.

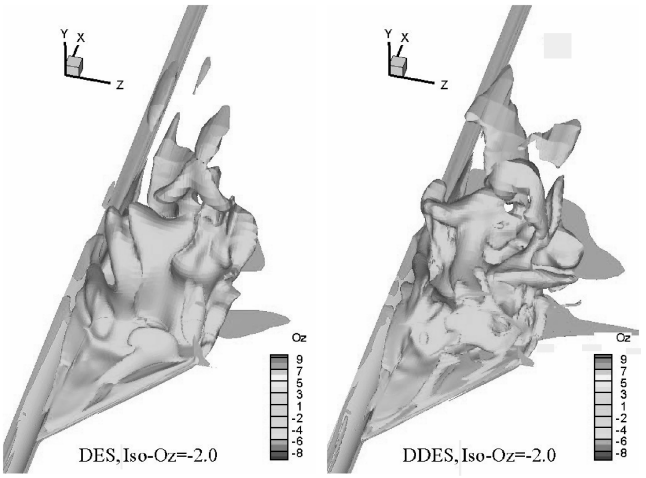

Fig. 16 Instantaneous vorticity isosurface ($\Omega_z = -2.0$).

Acknowledgements

This project is supported by the China Postdoctoral Science Foundation and the National Science Foundation of China under Contracts 10502030, 10477012, and 10232020, and the China NKBRSF Project 2001CB409600.

References

[1] Spalart, P. R., Jou, W.-H., Strelets, M., and Allmaras, S. R., "Comments on the Feasibility of LES for Wings, and on a Hybrid RANS/LES Approach," *Advanced in DNS/LES*, edited by C. Liu and Z. Liu, Greyden Press, Columbus, OH, Aug. 1997.

[2] Spalart, P. R., and Allmaras, S. R., "A One-Equation Turbulence Model for Aerodynamic Flows," AIAA Paper 92-0439, Jan. 1992.

[3] Strelets, M., "Detached Eddy Simulation of Massively Separated Flows," AIAA Paper 2001-0879, Jan. 2001.

[4] Menter, F. R., "Two-Equation Eddy-Viscosity Turbulence Models for Engineering Applications," *AIAA Journal*, Vol. 32, No. 8, 1994, pp. 1598–1605.

[5] Davidson, L., "Hybrid LES-RANS: A Comparison of a One-Equation SGS Model and a *k-l* Model for Prediction Recirculation Flows," *European Congress on Computational Methods in Applied Science and Engineering, Computational Dynamics Conference, 2001*, ECCOMAS, Swansea, Wales, U.K., Sept. 2001.

[6] Baurle, R. A., Tam, C.-J., Edwards, J. R., and Hassan, H. A., "Hybrid Simulation Approach for Cavity Flows: Blending, Algorithm, and Boundary Treatment Issues," *AIAA Journal*, Vol. 41, No. 8, 2003, pp. 1463–1480.

[7] Menter, F. R., and Kuntz, M., "A Zonal SST-DES Formulation," *DES-WORKSHOP*, July 2003 (http://cfd.me.umist.ac.uk/flomania/index2.html).

[8] Simon, F., Deck, S., Guillen, P., and Sagaut, P., "Hybrid RANS-LES Simulations of Supersonic Base Flow," *Symposium on Hybrid RANS/LES Methods, FOI*, edited by S.-H. Peng and W. Haase, 2005.

[9] Squires, K. D., Forsythe, J. R., Morton, S. A., Strang, W. Z., Wurtzler, K. E., Tomaro, R. F., Grismer, M. J., and Spalart, P. R., "Progress on Detached-Eddy Simulation of Massively Separated Flows," AIAA Paper 2002-1021, Jan. 2002.

[10] Forsythe, J. R., Hoffmann, K. A., Cummings, R. M., and Squires, K. D., "Detached-Eddy Simulation With Compressibility Corrections Applied to a Supersonic Axisymmetric Base Flow," *Journal of Fluids Engineering*, Vol. 124, No. 4, Dec. 2002, pp. 911–923.

[11] Viswanathan, A. K., Klismith, K. R., Forsythe, J. R., and Squires, K. D., "Detached-Eddy Simulation Around a Forebody at High Angle of Attack," AIAA Paper 2003-0263, Jan. 2003.

[12] Kotapati-Apparao, R. B., Squires, K. D., and Forsythe, J. R., "Prediction of the Flow over an Airfoil at Maximum Lift," AIAA Paper 2004-0259, Jan. 2004.

[13] Krishnan, V., Squires, K. D., and Forsythe, J. R., "Prediction of Separated Flow Characteristics over a Hump Using RANS and DES," AIAA Paper 2004-2224, July 2004.

[14] Constantinescu, G., and Squires, K. D., "Numerical Investigations of Flow over a Sphere in the Sub-Critical and Supercritical Regimes," *Physics of Fluids*, Vol. 16, No. 5, 2004, pp. 1449–1466.

[15] Wilcox, D. C., "Reassessment of the Scale-Determining Equation for

Advanced Turbulence Models," *AIAA Journal*, Vol. 26, No. 11, 1988, pp. 1299–1310.

[16] Fu, S., Rung, T., and Thiele, F., "Realizability of the Nonlinear Stress-Strain Relationships for Reynolds-Stress Closure," *Proceedings of the 11th Symposium on Turbulent Shear Flows*, Sep. 1997.

[17] Soo, H.-P., and Jang, H.-K., "Implementation of k-ω Turbulence Models in an Implicit Multigrid Method," *AIAA Journal*, Vol. 42, No. 7, 2004, pp. 1348–1357.

[18] Durbin, P. A., "On the k-ε Stagnation Point Anomaly," *International Journal of Heat and Fluid Flow*, Vol. 17, No. 1, 1996, pp. 89–90.

[19] Xiao, Z.-X., Chen, H.-X., Fu, S., and Li, F.-W., "Computations with k-g Model for Complex Configurations at High-Incidence," *Journal of Aircraft*, Vol. 42, No. 2, 2005, pp. 462–468.

[20] Runckel, J. F., and Lee, E. E., Jr., "Investigation at Transonic Speeds of the Loading over a 45 deg Sweptback Wing Having an Aspect Ratio of 3, a Taper Ratio of 0.2, and NACA 65A004 Airfoil Sections," NASA TN D-712, May 1961.

[21] Roe, P. L., "Approximate Riemann Solver, Parameter Vectors, and Difference Schemes," *Journal of Computational Physics*, Vol. 43, No. 2, 1981, pp. 357–372.

[22] Radespiel, R., and Swanson, R. C., "Progress with Multi-Grid Schemes for Hypersonic Flow Problems," NASA TR CR 189579, 1991.

[23] Li, J., Li, F.-W., and E, Q., "A Fully Implicit Method for Steady and Unsteady Viscous Flow Simulations," *Journal for Numerical Methods in Fluids*, Vol. 43, No. 2, 2003, pp. 147–163.

[24] Smagorinsky, J., "General Circulation Experiments with Primitive Equations. I. The Basic Experiment," *Monthly Weather Review*, Vol. 91, No. 3, 1963, pp. 99–164.

[25] Jameson, A., Schmidt, W., and Turkel, E., "Numerical Solutions of Euler Equations by Finite Volume Methods with Runge-Kutta Time Stepping Schemes," AIAA Paper 81-1259, June 1981.

[26] Yoon, S., and Jameson, A., "Lower-Upper Symmetric-Gauss-Seidel Method for the Euler and Navier-Stokes Equations," AIAA Paper 87-0600, Jan. 1987.